



SEISMIC COLLAPSE ANALYSIS OF RC FRAMED STRUCTURES USING THE GRADIENT INELASTIC FORCE-BASED ELEMENT FORMULATION

M. Salehi⁽¹⁾, P. Sideris⁽²⁾, A.B. Liel⁽³⁾

⁽¹⁾ Graduate Research Assistant, Dept. of Civil, Envir., and Arch. Eng., University of Colorado at Boulder, mosa6724@colorado.edu

⁽²⁾ Assistant Professor, Dept. of Civil, Envir., and Arch. Eng., University of Colorado at Boulder, petros.sideris@colorado.edu

⁽³⁾ Associate Professor, Dept. of Civil, Envir., and Arch. Eng., University of Colorado at Boulder, abbie.liel@colorado.edu

Abstract

This study assesses the capability of a novel force-based (FB) frame element – termed *gradient inelastic* (GI) FB element – to simulate the softening response and eventual collapse of a reinforced concrete (RC) framed structure. Although FB elements have been proven to be very efficient in predicting the hardening (pre-peak) response of framed structures, robust predictions of their softening response using FB elements have been hindered by strain softening phenomena that result in: (i) strain localization and loss of objectivity, and (ii) instabilities and failure of the numerical solution. The GI element has been formulated on the basis of a gradient inelastic beam theory and eliminates strain localization phenomena providing objective (mesh convergent) response and stability of the numerical solution. The GI element along with two other types of FB elements are employed to model a three-bay two-story RC moment frame. The other two FB elements incorporate end plastic hinge lengths through a plastic hinge integration method and are termed beam-with-hinges (BwH) elements herein. Both BwH elements use the so-called modified Gauss-Radau integration method. However, in the first BwH element, plasticity is solely introduced at the end sections (at the plastic hinge lengths), while, in the second BwH element, spread of plasticity is allowed by considering inelastic material response at all sections. Frame models generated with each modeling approach are analyzed using static pushover and Incremental Dynamic Analysis (IDA) and the predicted responses are compared in terms of pushover curves, IDA curves, and fragility curves for various limit states, including collapse. Although the models developed using the BwH elements predict pushover curves close to those obtained from the models generated with GI elements, BwH elements always underestimate damage (controlled by the peak strains), because the predicted peak strains by the BwH elements represent an average strain over the plastic hinge length. As a result, BwH elements predict systematically larger collapse capacities. On the contrary, the GI elements provide a deformation distribution over the entire member length, including the damage zones; hence, more accurately predicting peak responses. The GI elements were also found to provide stability of the numerical solution compared to all considered BwH elements.

Keywords: collapse analysis; reinforced concrete frames; softening response; gradient inelastic element; IDA.



1 Introduction

Performance-Based Earthquake Engineering (PBEE) requires accurate prediction of structural responses to different levels of earthquake dynamic loads up to complete collapse. This goal is only achievable if nonlinear models capable of simulating damage and failure of different structural components are available. This study focuses on the modeling of the softening response and damage of reinforced concrete (RC) members, whose response is dominated by axial-flexural interactions. Simulation of softening is essential for predicting the loss of strength that occurs due to the various physical mechanisms of damage, especially concrete spalling and crushing and rebar buckling.

To simulate the nonlinear response of RC framed structures, it is common to employ simplified models, such as two-node beam-columns elements, because use of continuum-based 3D finite element models [1, 2] is computationally expensive. Among the various types of elements, force-based (or flexibility-based, FB) elements are particularly popular for the analysis of members with hardening material models, because they can predict spreading of plasticity over their lengths, capture axial-flexural interactions, and exactly satisfy the force equilibrium and deformation compatibility. Force equilibrium is satisfied exactly, because the force shape functions are the solution to the equilibrium equations. Deformation compatibility is satisfied exactly, because the displacement field is obtained by direct integration of the strain-displacement equations [3, 4]. Even if the principle of virtual forces is employed to compute the displacement field, the solution would still be exact, because the virtual force field would be exact [5-7]. However, in the presence of softening materials, which are common in structural collapse simulations, conventional FB formulations suffer from the *strain localization* phenomenon [3, 4, 8, 9]. This phenomenon makes the post-peak responses of these elements highly sensitive to the number of the integration points (IPs) considered along their lengths, resulting in loss of objectivity in the predicted solution (i.e., divergence, instead of converge, with progressively increasing mesh refinements represented by an increasing number of IPs). This also leads to instabilities of the numerical solution algorithm – i.e., overshooting or trapping of the algorithm in “limiting cycles” between two or more solution trials, due to loss of the positive definiteness of the problem – and eventual convergence failure in the numerical solution [4, 5, 8, 10-13]. These problems have hindered the use of FB elements for the simulation of structural collapse. On the contrary, other, more simplified, approaches employing elements with softening end springs (concentrated plasticity elements) are widely used to account for softening phenomena, but require calibration with data from testing of structural members and components that experience softening to capture member response properties [14].

In this study, the capability of a novel FB element for the collapse simulation of RC frames is evaluated. This element, which is termed *gradient inelastic* (GI) FB frame element and has recently been formulated by the authors [4, 9], has been shown to be capable of alleviating the aforementioned deficiencies of conventional FB elements.

2 Current Modeling Approaches for Collapse Analysis

Researchers have suggested a variety of modeling approaches to simulate the response of flexure-critical RC members under extreme deformations, among which, three are more commonly employed: (i) using elastic linear beam-column elements with nonlinear zero-length springs at the ends (e.g., [15-17]), (ii) using FB beam-column elements with plastic hinges of prescribed length at the ends – herein termed *beam-with-hinges* (BwH) elements – with or without plasticity spreading (e.g., [18-20]), and (iii) using a set of displacement-based (DB) beam-column elements in series to represent a single RC beam-column (e.g., [18, 21]). Each of these approaches suffer from their own particular drawbacks, as discussed below.

The first approach indirectly accounts for physical phenomena associated with softening, such as concrete spalling and crushing, rebar buckling and bar slip, by using phenomenological spring models calibrated to macroscopic experimental data (forces/moments and displacements/rotations) from member and component testing studies. This approach does not separate between effects caused by individual damage mechanisms on the observed response, since all damage mechanisms are integrated into a single rotational nonlinear spring. Also, this approach cannot predict spread of plasticity over the beam-column length, which is particularly important



for members subject to reverse lateral loads and distributed gravity loads. Moreover, this approach does not account for the axial-flexural interactions, which are significant for columns subjected to large axial force variations due to gravity loads and overturning effects.

The second approach, despite being capable of predicting the spread of plasticity over the beam-column length, suffers from other limitations and deficiencies. There are mainly two types of BwH elements in terms of the selected plastic hinge integration method: (1) those using the so-called *modified Gauss-Radau* integration method [10], and (2) those using the so-called *regularized hinge* integration method [22]. Because of the fixed number of six integration points, the modified Gauss-Radau integration method leads to inaccurate hardening responses [10, 22], a challenge partly addressed by the regularized hinge integration method [22]. Also, because of the requirement for a fixed number of six IPs in the modified Gauss-Radau integration method, examination of section strain distributions over the member length are hindered and mesh-refinement convergence studies at the element level are not possible. Furthermore, the modified Gauss-Radau integration method introduces limitations on the length of the element, which should be larger than $4 \times (l_{pI} + l_{pJ})$, where l_{pI} and l_{pJ} are the plastic hinge lengths at the two ends, because otherwise the integration weights of its two middle IPs become negative, so that the sum of all integration weights does not exceed 1. Such negative integration weights, cause instabilities and convergence failures (similarly to the instabilities of Newton-Cotes quadrature for large number of points, e.g., 19 or 20). Negative weights often occur in the case of the regularized hinge integration, which needs selection of two additional parameters, ζ_I and ζ_J . These parameters are difficult to calibrate, because they are properties of the integration scheme, rather than physical properties of the member or the material models. Analyses conducted as part of this research have further shown that BwH elements using the regularized hinge integration method may suffer from severe instabilities and convergence failures of the numerical solution at the onset of softening, which makes them unsuitable for the collapse analysis of RC frames.

The third approach still suffers from localization and loss of objectivity; however, localization now occurs at individual (displacement-based) elements, rather than integration points, because the strain field is prescribed over the entire element length. Thus, increasing the number of elements results in a progressively more localized response [23]. Displacement-based elements violate force equilibrium over the element length [5, 7]. Moreover, discretization of each structural member into a number of displacement-based elements (three to five, at minimum) significantly increases the number of degrees of freedom of the structural model and the computational effort.

3 Gradient Inelastic Force-Based Frame Element

Given these limitations, development of modeling strategies without the shortcomings of the currently used approaches is crucial to the accurate evaluation of the response of RC frames under intense earthquake shaking. To address these challenges, the GI frame element formulation [4, 9] was recently proposed. The GI formulation is based on a novel GI beam theory that alleviates strain localization during strain softening by introducing a set of gradient nonlocality relations between nonlocal and local section strains and replacing local section strains with their nonlocal counterparts in the strain-displacement equations. The GI beam theory and element formulation ensure continuous and bounded section strain distributions, and objective (mesh convergent) response. Specifically, the GI element formulation has been shown to generate objective nodal force-displacement and section force-strain responses in the presence of softening section constitutive relations, under both monotonic and random reverse loadings.

Unlike other formulations (e.g., [8, 13]), the GI element formulation does not restrict the form/type of the considered material constitutive relations. The only additional parameter needed to define this element is a *characteristic length*, which controls the spread of plasticity and represents the plastic hinge length. The GI element formulation reduces to the conventional (local) FB formulation if this characteristic length is chosen to be zero. Moreover, the GI element provides predictions of the section strain distributions over the member length (with desirable resolution), converges with the number of integration points, and does not have the aforementioned limitations of the BwH elements in terms of element length and the number of IPs.



4 Scope

In this study, three types of FB elements are employed to model a RC moment-resisting frame: (i) BwH elements with concentrated plasticity at the ends, (ii) BwH elements with plasticity spreading, and (iii) GI elements. For all BwH elements, the modified Gauss-Radau integration method is considered. For the first BwH element, all sections, except for the end ones, are assumed to have linear elastic response, whereas for the second BwH element and the GI element, all sections incorporate inelastic (softening) constitutive relations. The frame modeled by the three above elements is analyzed using both the nonlinear static (pushover) analysis method and the Incremental Dynamic Analysis (IDA) method [24, 25]. The results of these analyses are translated into pushover curves, IDA curves, and fragility curves, and compared for the three modeling approaches.

5 Archetype RC Frame

The archetype RC frame examined here is the three-bay two-story frame shown in Fig. 1, which was selected from the moment frames designed by Haselton [26] – with ID of 1001 per [26]. This frame was designed per 2003 IBC [27], ASCE 7-02 [28], and ACI 318-02 [29], for a highly seismic site in California and meets the requirements of the special moment resisting frames. The frame used for analysis is the interior frame indicated in Fig. 1 (a). Each bay spans 20 ft, while the heights of the first and the second stories are 15 ft and 13 ft, respectively (Fig. 1 (b)). All the columns have 22×22 in² square cross sections, while all the beams have rectangular cross sections with width of 22 in. and height of 18 in. The slab thickness is 8 in. The details of the longitudinal and transverse reinforcements can be found elsewhere [26]. The nominal strength of concrete is 5 ksi, and the yield strength of steel reinforcement is 60 ksi.

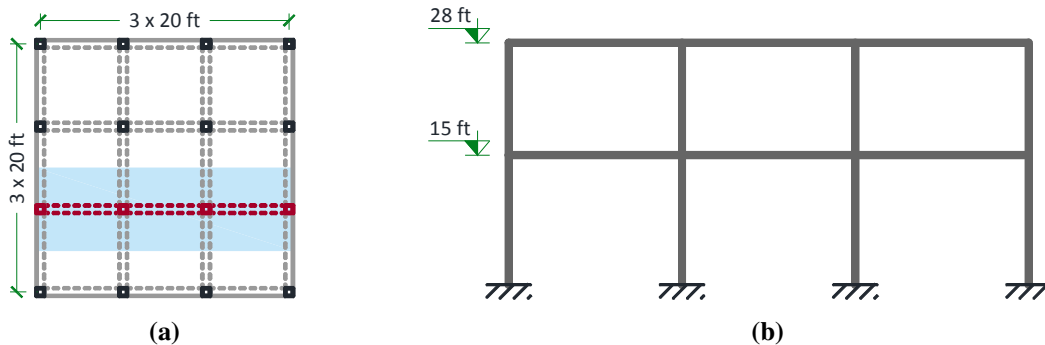


Fig. 1 – (a) Frame location in building plan; (b) frame elevation

6 Modeling Approaches

In order to use the GI element to simulate the archetype RC frame, the GI formulation was implemented by the authors in the structural analysis software OpenSees [30]. The BwH element was already available in the OpenSees element library. Because the purpose of this study is to examine the capability of GI elements (compared to other formulations) to capture the axial-flexural failure of RC beam-columns solely driven by softening material relations, other damage mechanisms contributing to collapse, such as bond-slip effects, are not incorporated in the models. The generic element configuration employed to simulate the archetype RC frame is illustrated in Fig. 2. The *Modeling Approaches* 1, 2, and 3 correspond to BwH with concentrated plasticity, BwH with plasticity spreading, and GI, respectively. In all *Modeling Approaches*, the plastic hinge lengths are assumed to be equal to the member cross section depths. The beam-to-column joint panel zones are modeled by rigid links connecting the centerline nodes to the connection interface nodes. The corotational geometric transformation is used to account for the large deformation effects. The columns are assumed to be fixed to the foundation.

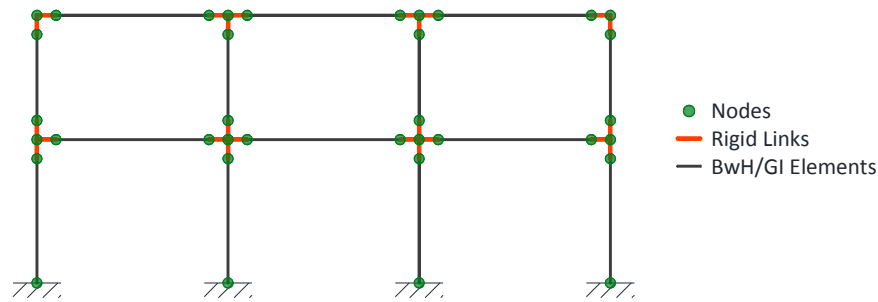


Fig. 2 – Generic element configuration for frame models

The strength and stiffness contributions of the slabs are taken into account by considering their effective widths in the definition of the beam sections. The effective slab widths are selected to be equal to $\frac{1}{4}$ of the beam spans [29], i.e. 5 ft. The GI elements representing beams and columns incorporate 19 and 15 IPs, respectively, to guarantee converged response [4, 9], while each BwH element has the fixed number of 6 IPs. All sections along the beam-column elements in *Modeling Approaches 2* and *3* are defined as fiber sections with softening uniaxial response for the concrete material and steel reinforcement. For *Modeling Approach 1*, only the end sections of the BwH elements use fiber discretization with softening material response, while the interior sections use linear elastic material models. The schematic discretization of the fiber sections for the columns and beams are shown in Figs. 3 (a) and (b), respectively. Each fiber section includes three groups of fibers: (i) confined (core) concrete, (ii) unconfined (cover) concrete, and (iii) longitudinal steel rebar.

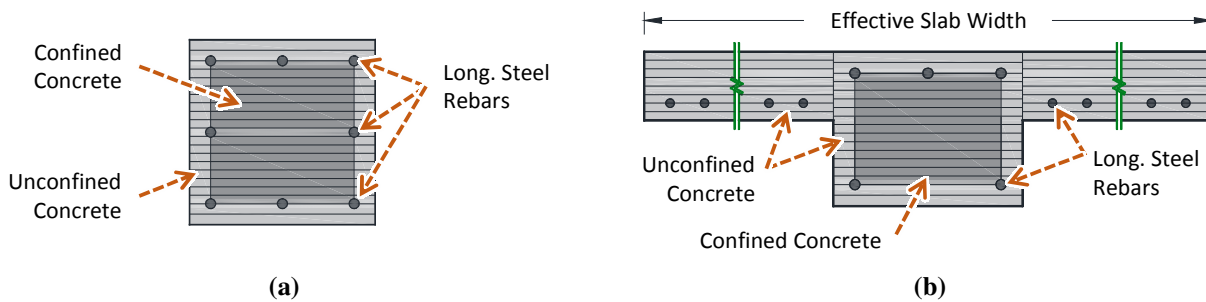


Fig. 3 – Schematic discretization of: (a) column fiber sections; (b) T-beam fiber sections

The properties of the confined concrete materials in each beam/column section and their uniaxial stress-strain relationships are determined in accordance with the Mander’s model [31]. The uniaxial stress-strain relationship for the longitudinal steel is defined according to the Giuffré-Menegotto-Pinto model [32] with a strain hardening ratio of 1%. The Giuffré-Menegotto-Pinto model was further modified in this study to incorporate strength and stiffness deterioration/fracture through implementation of a damage reduction factor. This factor linearly varies from 1, for the maximum experienced strain of 0.09 [33], to 0.01, for the maximum experienced strain of 0.1. The responses of the linear elastic sections are defined based on the cracked concrete properties [26], using the reduction factors of 0.35 and 0.7 for the moments of inertia of the beams and the columns, respectively [29]. The gravity loads and the translational and rotational seismic masses are assigned as point loads and lumped masses, respectively, to the nodes along the floor centerlines.

7 Eigenvalue Analysis

According to the eigenvalue analysis of the frame modeled using either one of *Modeling Approaches 2* or *3*, the periods of vibration of the first two modes are 0.294 and 0.091 sec., respectively. Note that these periods are larger for the frame modeled using *Modeling Approach 1* (0.350 and 0.105 sec.) because of the use of cracked section properties for the elastic sections.



8 Pushover Analysis

Nonlinear static pushover analyses are performed using two different distributed load patterns: (1) proportional to the frame’s first mode shape, and (2) uniform over the frame’s height. The base shear versus roof lateral displacement (and roof lateral drift ratio) responses of the archetype frame obtained from the pushover analyses using the aforementioned *Modeling Approaches* are compared in Fig. 4, while interstory shears vs. interstory drifts (and drift ratios) are shown in Fig. 5. The responses obtained from the first two *Modeling Approaches* are almost identical. This similarity is present because, for the modified Gauss-Radau integration method, the interior IPs are located far from the end IPs (at least at a distance of $8 \cdot l_p/3$), thereby, remaining almost elastic at all times, even for *Modeling Approach 2*. For all load patterns, the post-peak response is dominated by failure of the first story (soft story). The peak base shear forces predicted by the three models are nearly identical. Because of the soft story failure mechanism, the uniform load pattern is more representative of the seismically-induced dynamic load, for which, *Modeling Approach 3* predicts more rapid softening.

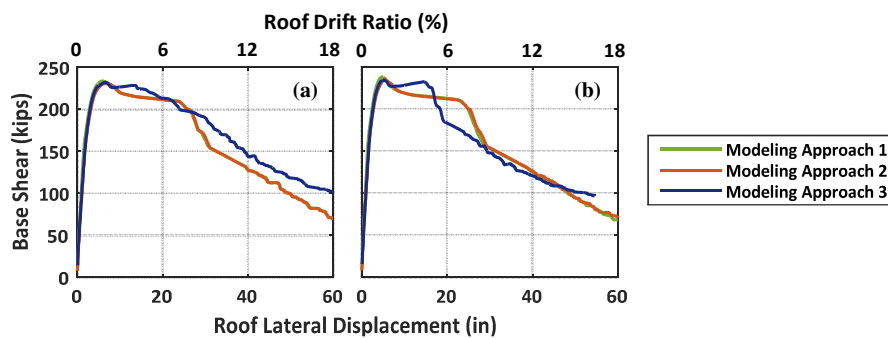


Fig. 4 – Pushover analysis results – Base shear vs. roof lateral displacement/drift ratio obtained using: (a) load pattern proportional to frame’s first mode shape; and (b) uniform load pattern

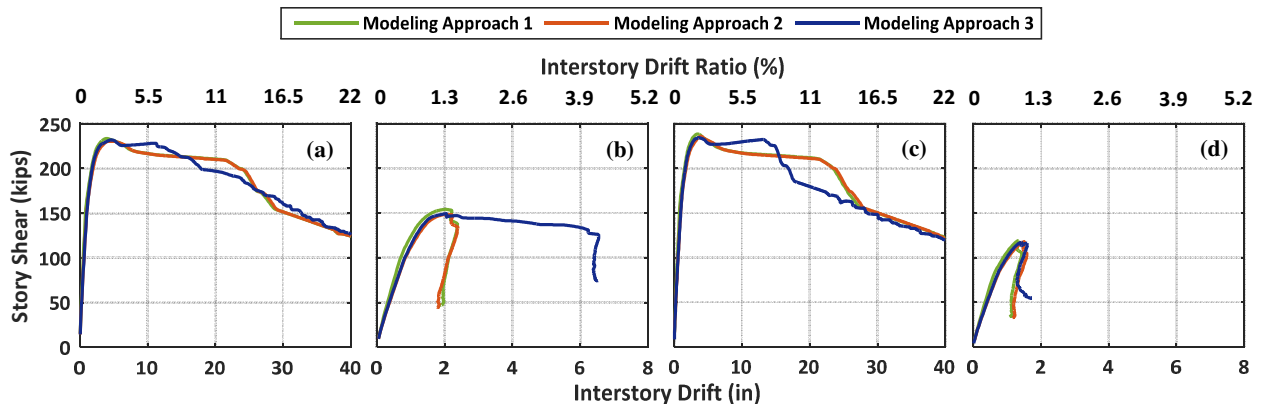


Fig. 5 – Pushover analysis results – Interstory shear vs. interstory drift (and drift ratio): (a) first story and load pattern proportional to frame’s first mode shape; (b) second story and load pattern proportional to frame’s first mode shape; (c) first story and uniform load pattern; and (d) second story and uniform load pattern

9 Dynamic Analysis

9.1 Analysis Methodology

Time-history analyses are run using the average acceleration Newmark’s integration method. Damping ratios of 2% of the critical damping are assigned to the first two modes of the frame, using the Rayleigh method and updated based on tangent stiffnesses throughout the analysis to avoid unrealistically large damping forces during softening. The FEMA P695 far-field ground motion set [34] is used to perform the IDAs, adding in the vertical



components to the records in the original set. One ground motion is excluded because the vertical acceleration component is not available. Information on these 21 ground motion pairs is summarized in Table 1. All of these ground motions have peak ground accelerations larger than 0.2g, peak ground velocities larger than 15 cm/sec., and are from earthquakes with magnitudes greater than 6.5, which make them suitable for collapse analysis.

Table 1 – Ground-motion information

No.	Earthquake			Recording Station	
	M	Year	Name	Name	Owner
1	6.7	1994	Northridge	Beverly Hills - Mulhol	USC
2	6.7	1994	Northridge	Canyon Country-WLC	USC
3	7.1	1999	Duzce, Turkey	Bolu	ERD
4	7.1	1999	Hector Mine	Hector	SCSN
5	6.5	1979	Imperial Valley	Delta	UNAMUCSD
6	6.5	1979	Imperial Valley	El Centro Array #11	USGS
7	6.9	1995	Kobe, Japan	Nishi-Akashi	CUE
8	6.9	1995	Kobe, Japan	Shin-Osaka	CUE
9	7.5	1999	Kocaeli, Turkey	Duzce	ERD
10	7.5	1999	Kocaeli, Turkey	Arcelik	KOERI
11	7.3	1992	Landers	Yermo Fire Station	CDMG
12	7.3	1992	Landers	Coolwater	SCE
13	6.9	1989	Loma Prieta	Capitola	CDMG
14	6.9	1989	Loma Prieta	Gilroy Array #3	CDMG
15	7.4	1990	Manjil, Iran	Abbar	BHRC
16	6.5	1987	Superstition Hills	El Centro Imp. Co.	CDMG
17	7	1992	Cape Mendocino	Rio Dell Overpass	CDMG
18	7.6	1999	Chi-Chi, Taiwan	CHY101	CWB
19	7.6	1999	Chi-Chi, Taiwan	TCU045	CWB
20	6.6	1971	San Fernando	LA - Hollywood Stor	CDMG
21	6.5	1976	Friuli, Italy	Tolmezzo	--

The time-history analyses are conducted by applying each of the horizontal components together with the corresponding vertical component of the ground motion acceleration records (giving a total of 42 pairs of acceleration records). To capture residual displacements, analyses are continued for 10 sec., after the ground motions finish, to ensure the frame comes to rest. The 5%-damping acceleration response spectra for the 42 horizontal components of the selected ground motions and their geometric mean are shown in Fig. 6. The geometric mean spectral acceleration at the fundamental period of the frame, $Sa_{g.m.}(T_1, 5\%)$, is used as the intensity measure, IM , for scaling the ground motions in the IDAs.

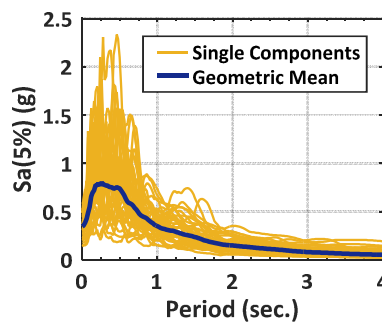


Fig. 6 – Response acceleration spectra for horizontal components of ground motions

Each IDA is conducted by scaling records to increasing intensity, each time simulating dynamic structural response. An IDA using each pair of (horizontal and vertical) acceleration records is stopped when residual interstory drift ratio of any story exceeds 30% for three consecutive scaling factors. For residual interstory drift ratios exceeding 30%, the frame is assumed to have already collapsed, as discussed later. For the developed

models, the numerical solution algorithm did not exhibit numerical instabilities or convergence failures and could capture the response up to large interstory drift ratios (e.g., 50% or larger) and any of the potential failure mechanisms (Fig. 7).

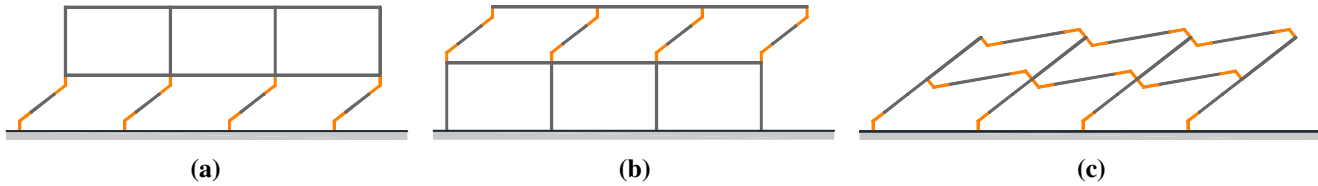


Fig. 7 – Illustration of major possible frame collapse modes

9.2 Results and Discussion

9.2.1 Single Analysis

Before looking into the IDA results, the response of the frame under a single strong motion is examined using the different *Modeling Approaches*. The acceleration records used for this purpose are the 090 and the vertical components of the San Fernando motion in Table 1, with a scale factor of 5.5. The roof lateral displacement responses obtained from the three models are compared in Fig. 8 (a). The responses obtained from *Modeling Approaches 1* and 2 have minimal differences, while the response obtained from *Modeling Approach 3* resembles them just up to the time instant when the peak negative displacement is achieved (at $t \approx 8$ sec.). Following this time instant, the response obtained using *Modeling Approach 3* shows larger peak values in the positive direction, which implies that this model predicts larger damage for the frame. The curvature distributions over the left external column of the first story at the time instants when the peak negative and positive displacements occur (labeled as t_a and t_b in Fig. 8 (a)) are compared in Fig. 8 (b). The curvature distributions obtained from the first two *Modeling Approaches* are almost identical, while *Modeling Approach 3* leads to larger curvatures at the column ends. The reason why *Modeling Approaches 1* and 2 predict smaller curvatures for the bottom section (the critical section for the considered column) is that in the BwH elements, the section strains are assumed to be constant over the entire plastic hinge lengths, hence, providing an estimate of the “average” strain over the damage zone (plastic hinge). On the contrary, the GI element provides a prediction of the distribution of strains over the entire element length, including the damage zones, which is in agreement with experimental observations.

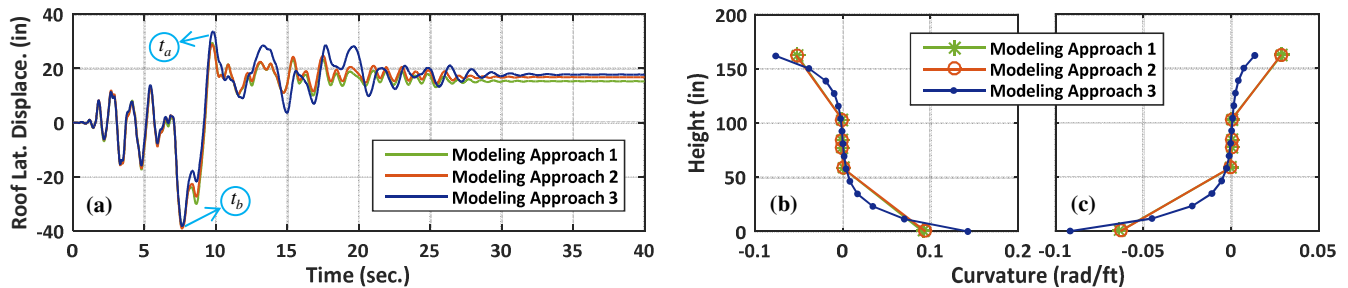


Fig. 8 – Single time-history analysis results – (a) Roof lateral displacement vs. time; (b) curvature distributions along an external column at t_a ; and (c) curvature distributions along an external column at t_b

9.2.2 Incremental Dynamic Analysis

The results obtained from the IDAs are translated into (a) IDA curves, showing *IM* vs. engineering demand parameters (*EDPs*), and (b) fragility curves for various limit states (*LSs*) on the selected *EDPs*, representing various levels of physical damage. The *EDPs* selected for this study are: (i) peak interstory drift ratio (*PIDR*), (ii) residual interstory drift ratio (*RIDR*), (iii) peak roof drift ratio (*PRDR*), (iv) peak floor acceleration (*PFA*), (v)

peak cover concrete compressive strain, $\epsilon_{c,cover}^{peak}$, (vi) peak core concrete compressive strain, $\epsilon_{c,core}^{peak}$, and (vii) peak longitudinal steel bar strain, ϵ_s^{peak} . The concrete and the longitudinal steel bar strains are recorded in different locations of the two end cross sections of each member, as shown Fig. 9.

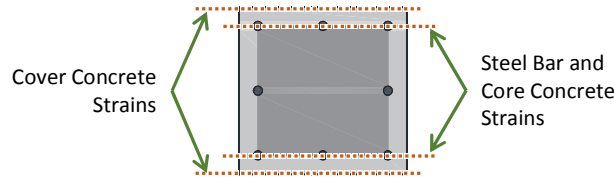


Fig. 9 –Member end cross sections showing strain recording locations.

Three *LSs* were considered for the *RIDR*, representing: (I-1) slight damage, (I-2) moderate damage, (I-3) extensive damage. Also, two *LSs* were for the concrete material EDPs, representing: (II-1) spalling of the cover concrete, and (II-2) crushing of the core concrete. Finally, three *LSs* were considered for the peak longitudinal steel bar strain, representing: (III-1) longitudinal steel bar yielding, (III-2) longitudinal steel bar buckling, and (III-3) longitudinal steel bar fracture. All *LSs* for the selected EDPs are summarized in Table 2, where ϵ_{spall} , ϵ_{cu} , and ϵ_{bb} are concrete spalling strain, concrete crushing strain, and longitudinal bar buckling strain, respectively, which vary for different cross sections, based on their spatial and mechanical properties. Frame collapse is assumed for *RIDR* > 20%, which represents a 20% reduction of the interstory shear (from its overall peak value) in the post-peak range (Fig. 5).

Table 2 – *LSs* for the selected EDPs

ID	Physical Damage	Related EDP	LS	Reference
I-1	Slight-damage residual drift	<i>RIDR</i>	0.5%	[35]
I-2	Moderate-damage residual drift	<i>RIDR</i>	1%	[35]
I-3	Extensive-damage residual drift	<i>RIDR</i>	4.6%	[35]
II-1	Concrete cover spalling	$\epsilon_{c,cover}^{peak}$	ϵ_{spall}	[36]
II-2	Concrete core crushing	$\epsilon_{c,core}^{peak}$	ϵ_{cu}	[31]
III-1	Longitudinal steel bar yielding	ϵ_s^{peak}	0.0023	[33]
III-2	Longitudinal steel bar buckling	ϵ_s^{peak}	ϵ_{bb}	[36]
III-3	Longitudinal steel bar fracture	ϵ_s^{peak}	0.09	[33]

The median, 16% percentile and 84% percentile IDA curves are shown in Fig. 10 for all *Modeling Approaches*. For all models, the median IDAs (excluding the curves related to the *PFA*s) flatline at a $Sa_{g,m}$ larger than 7.5 g, which is slightly larger than the predictions by Haselton [26], most probably because bond-slip effects were neglected. The IDA curves resulted from *Modeling Approaches* 1 and 2 are very close (except for those referring to *PFA*s), which indicates that using linear elastic section force-deformation relationships for the interior sections of the BwH elements in *Modeling Approach* 1 does not significantly affect the displacement-related EDPs. At the same *IMs*, however, the *PFA*s resulted from *Modeling Approach* 2 are almost twice those obtained by using *Modeling Approach* 1. The IDA curves achieved with *Modeling Approach* 3 resemble those obtained from *Modeling Approaches* 1 and 2 before the curves become flat, but show about 20% smaller *IMs* for the intensity at which flatlines are observed. The *PFA*s predicted by this model are, however, close to those obtained by using *Modeling Approach* 2, with slightly larger record-to-record dispersion.

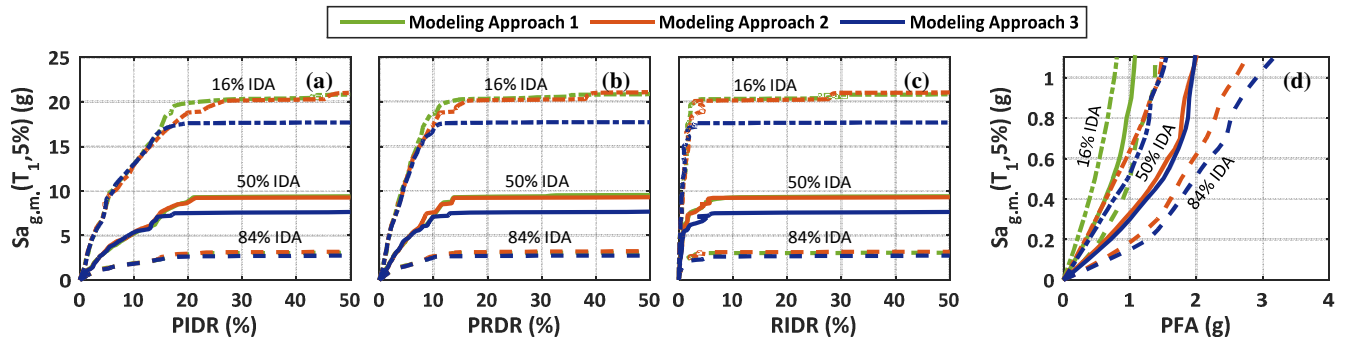


Fig. 10 – IDA results – $Sa_{g,m}(T_1, 5\%)$ vs.: (a) peak interstory drift ratio; (b) peak roof drift ratio; (c) residual interstory drift ratio; and (d) peak floor acceleration.

The fragility curves – showing the cumulative probability of an *EDP* exceeding a *LS* at any *IM*, $P(EDP > LS | IM)$ – are generated based on the *LSs* of Table 2 and assuming that the IDA results follow lognormal distributions [34, 35]. The collapse fragility curves (i.e., fragility curves for the $RIDR > 20\%$) and the fragility curves related to the other *EDPs* are shown in Fig. 11. Fragility curves related to concrete and steel rebar strains are examined only for the columns of the first story, which were found to always sustain the most severe damages. According to Fig. 11 (a), the median *IMs* at which frame collapse occurs are $Sa_{g,m} = 10.2, 9.5,$ and 7.8 g, for *Modeling Approaches* 1, 2, and 3, respectively. Nearly identical collapse fragility curves are obtained for $PIDR > 20\%$, because at collapse, peak and residual drifts are nearly identical. *Modeling Approaches* 1 and 2 predict larger collapse capacities compared to *Modeling Approach* 3, by 35% and 22%, respectively. Similar observations can be made for the remaining *EDPs*, particularly for those *LSs* exceeded after the RC frame experiences softening (i.e., I-3, II-1, II-2, III-2, and III-3). This observation is associated with the fact that the GI formulation always predicts larger strains at the damage zones, compared to the BwH formulations, which predicts an average strain over the damage zone (plastic hinge).

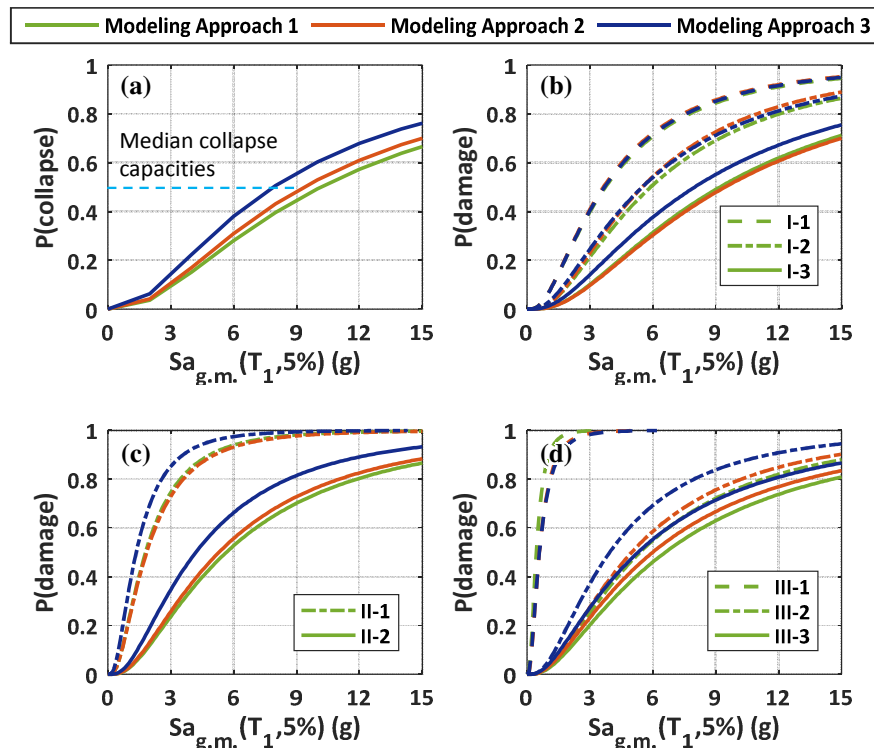


Fig. 11 – IDA results – Fragility curves for: (a) collapse; (b) damage based on residual drift *LSs*; (c) damage based on 1st story internal column *LSs* related to concrete; (d) damage based on 1st story internal columns related to longitudinal steel bars



10 Summary and Conclusions

The recently introduced GI flexibility-based element formulation [4, 9] was evaluated in the framework of collapse analysis of RC frames through comparison with two versions of FB elements incorporating plastic hinge integration techniques and termed BwH elements herein. These two BwH elements and the GI element were used to model a three-bay two-story RC moment-resisting frame. The frame was analyzed under static pushover and dynamic earthquake loads. Specific findings of this research include:

- The model developed using the GI elements was capable of simulating softening and collapse in RC frames, by capturing large peak and residual interstory drift ratios, without numerical instabilities and convergence failures prevalent in models employing conventional FB elements. The GI elements can be implemented as typical FB elements, because they only introduce a single additional model parameter, the *characteristic length*, which represents the plastic hinge length and is usually taken as the cross-section depth.
- Use of the GI elements allows examination of strain distributions over the length of the RC member with the desired resolution and at any level of member deformations. Peak curvatures obtained using the GI element are generally larger than those obtained from BwH elements, because BwH elements assume an *average* strain distribution over the plastic hinge length, rather than solving for the *actual* strain distribution via a suitable beam theory addressing localization phenomena. As a result, the models with BwH elements overestimated the collapse capacity of the considered RC frame, predicting larger median collapse capacities by 20% to 30%.
- The exercise of comparing these frame models also shows that, given the small (and fixed) number of six integration points utilized in the BwH elements with Gauss-Radau integration and their locations, inelastic response is mostly limited to the end sections of the BwH element, not allowing spread of plasticity. Also, the selection of the plastic hinge lengths is not free, and, often, physically admissible and reasonable plastic hinge lengths can generate *negative* integration weights resulting in instability and convergence failures of the numerical solution.

11 Acknowledgements

Financial support for this research has been partly provided by the National Science Foundation (NSF) under grant # CMMI 1538585. This support is gratefully acknowledged. The opinions, findings, and the conclusions presented in this paper belong to the authors and do not necessarily reflect the views of the NSF.

12 References

- [1] Luccioni, B.M., R.D. Ambrosini, and R.F. Danesi (2004): Analysis of Building Collapse under Blast Loads. *Engineering Structures*, **26**: 63-71.
- [2] Hansen, E., et al. (2006): Computational Failure Analysis of Reinforced Concrete Structures Subjected to Blast Loading. *17th Analysis and Computation Specialty Conferenc at Structures Congress*. St. Louis, MO, USA.
- [3] Sideris, P. (2012): Seismic Analysis and Design of Precast Concrete Segmental Bridges. *Ph.D. Thesis*, Department of Civil, Structural, and Environmental Engineering, University at Buffalo,
- [4] Sideris, P. and M. Salehi (2016): A Gradient Inelastic Flexibility-Based Frame Element Formulation. *Journal of Engineering Mechanics*. DOI: 10.1061/(ASCE)EM.1943-7889.0001083.
- [5] Zeris, C. and S. Mahin (1988): Analysis of Reinforced Concrete Beam-Columns under Uniaxial Excitation. *Journal of Structural Engineering*, **114**(4): 804-820.
- [6] Kunnath, S.K., A.M. Reinhorn, and Y.J. Park (1990): Analytical Modeling of Inelastic Seismic Response of R/C Structures. *Journal of Structural Engineering*, **116**(4): 996-1017.
- [7] Taucer, F., E. Spacone, and F.C. Filippou (1991): A Fiber Beam-Column Element for Seismic Response Analysis of Reinforced Concrete Structures. *Technical Report UCB/EERC-91/17*, Earthquake Engineering Research Center, Berkeley, CA, USA.
- [8] Coleman, J. and E. Spacone (2001): Localization Issues in Force-Based Frame Elements. *Journal of Structural Engineering*, **127**(11): 1257-1265.
- [9] Salehi, M. and P. Sideris (2016): Refined Gradient Inelastic Flexibility-Based Formulation for Members Subjected to Random Reverse Loading. *Journal of Engineering Mechanics (under review)*.



- [10] Scott, M.H. and G.L. Fenves (2006): Plastic Hinge Integration Methods for Force-Based Beam-Column Elements. *Journal of Structural Engineering*, **132**(2): 244-252.
- [11] Addessi, D. and V. Ciampi (2007): A Regularized Force-Based Beam Element with a Damage-Plastic Section Constitutive Law. *International Journal for Numerical Methods in Engineering*, **70**: 610-629.
- [12] Almeida, J.P., S. Das, and R. Pinho (2012): Adaptive Force-Based Frame Element for Regularized Softening Response. *Computers and Structures*, **102-103**: 1-13.
- [13] Valipour, H.R. and S.J. Foster (2009): Nonlocal Damage Formulation for a Flexibility-Based Frame Element. *Journal of Structural Engineering*, **135**(10): 1213-1221.
- [14] Haselton, C.B., A.B. Liel, and G.G. Deierlein (2009): Simulating structural collapse due to earthquakes: model idealization, model calibration, and numerical solution algorithms. *Computational Methods in Structural Dynamics and Earthquake Engineering (COMPdyn)*.
- [15] Elwood, K.J. and J.P. Moehle (2003): Shake Table Tests and Analytical Studies on the Gravity Load Collapse of Reinforced Concrete Frames. *Technical Report PEER 2003/01*, Pacific Earthquake Engineering Research Center, Berkeley, CA, USA.
- [16] Haselton, C.B., et al. (2011): Seismic Collapse Safety of Reinforced Concrete Buildings: I. Assessment of Ductile Moment Frames. *Journal of Structural Engineering*, **137**(4): 481-491.
- [17] Goulet, C.A., et al. (2007): Evaluation of the Seismic Performance of a Code-Conforming Reinforced-Concrete Frame Building—from Seismic Hazard to Collapse Safety and Economic Losses. *Earthquake Engineering and Structural Dynamics*, **36**: 1973-1997.
- [18] Talaat, M.M. and K.M. Mosalam (2008): Computational Modeling of Progressive Collapse in Reinforced Concrete Frame Structures. *Technical Report PEER 2007/10*, Pacific Earthquake Engineering Research Center, Berkeley, CA, USA.
- [19] Feng, D., et al. (2015): Collapse Simulation of Reinforced Concrete Frame Structures. *The Structural Design of Tall and Special Buildings*. DOI: 10.1002/tal.1273.
- [20] Vidot-Vega, A. and M. Kowalsky (2013): Drift, Strain Limits and Ductility Demands for RC Moment Frames Designed with Displacement-Based and Force-Based Design Methods. *Engineering Structures*, **51**: 128-140.
- [21] Erberik, M.A. and A.S. Elnashai (2004): Fragility Analysis of Flat-Slab Structures. *Engineering Structures*, **26**: 937-948.
- [22] Scott, M.H. and O.M. Hamutcuoglu (2008): Numerically Consistent Regularization of Force-Based Frame Elements. *International Journal for Numerical Methods in Engineering*, **76**: 1612-1631.
- [23] Calabrese, A., J.P. Almeida, and R. Pinho (2010): Numerical Issues in Distributed Inelasticity Modeling of RC Frame Elements for Seismic Analysis. *Journal of Earthquake Engineering*, **14**(S1): 38-68.
- [24] Vamvatsikos, D. and C.A. Cornell (2002): Incremental Dynamic Analysis. *Earthquake Engineering and Structural Dynamics*, **31**: 491-514.
- [25] Vamvatsikos, D. and C.A. Cornell (2004): Applied Incremental Dynamic Analysis. *Earthquake Spectra*, **20**(2): 523-553.
- [26] Haselton, C.B. (2006): Assessing Seismic Collapse Safety of Modern Reinforced Concrete Moment Frame Buildings. *Ph.D. Thesis*, Department of Civil and Environmental Engineering, Stanford University, CA, USA.
- [27] International Code Council, I. (2003): 2003 International Building Code (IBC) Country Club Hills, IL, USA.
- [28] American Society of Civil Engineers (2002): Minimum Design Loads for Buildings and Other Structures (ASCE7-02). Reston, VA, USA.
- [29] American Concrete Institute (2002): Building Code Requirements for Structural Concrete and Commentary (ACI 318-02). Farmington Hills, MI, USA.
- [30] McKenna, F., G.L. Fenves, and M.H. Scott (2000): Open System for Earthquake Engineering Simulation. Pacific Earthquake Engineering Research Center: Berkeley, CA, USA.
- [31] Mander, J.B., M.J.N. Priestley, and R. Park (1988): Theoretical Stress-Strain Model for Confined Concrete. *Journal of Structural Engineering*, **114**: 1804-1826.
- [32] Giuffrè, A. and P.E. Pinto (1970): Il comportamento del cemento armato per sollecitazioni cicliche di forte intensità. *Giornale del Genio Civile*, **5**(1): 391-408.
- [33] Caltrans (2013): Caltrans Seismic Design Criteria CA, USA.
- [34] Applied Technology Council (2009): Quantification of Building Seismic Performance Factors (FEMA P695). *Federal Emergency Management Agency*, Washington, DC, USA.
- [35] Applied Technology Council (2012): Seismic Performance Assessment of Buildings Volume 1 – Methodology (FEMA P-58-1). *Federal Emergency Management Agency*, Washington, DC, USA.
- [36] Berry, M. and M. Eberhard (2003): Performance Models for Flexural Damage in Reinforced Concrete Columns. *Technical Report PEER 2003/18*, Pacific Earthquake Engineering Research Center, Berkeley, CA, USA.